The Astronomical Journal, 170:241 (7pp), 2025 October https://doi.org/10.3847/1538-3881/ae0585

The DELVE Quadruple Quasar Search. I. A Lensed Low-luminosity Active Galactic Nucleus

Paul L. Schechter[1], Dominique Sluse[2], Erik A. Zaborowski[3,4,5], Alex Drlica-Wagner[5,6,7], Cameron Lemon[8], Frederic Dux[8,9], Frederic Courbin[8,10,11], Angela Hempel[12,13], Martin Millon[8,14,15], Tommaso Treu[16], Raul Teixeira[7], Monika Adamów[17], Clecio R. Bom[18], Julio A. Carballo-Bello[19], Peter S. Ferguson[20], Robert A. Gruendl[17], David J. James[21,22], Clara E. Martínez-Vázquez[23], Pol Massana[24], Sidney Mau[14,15], Burçin Mutlu-Pakdil[25], Noëlia E. D. Noël[26], Andrew B. Pace[27], Joanna D. Sakowska[26], Guy S. Stringfellow[28], Erik J. Tollerud[29], A. Katherina Vivas[30], and Alfredo Zenteno[30]
[1] MIT Kavli Institute and Department of Physics, 77 Massachusetts Ave., Cambridge, MA 02139, USA; schech@mit.edu
[2] STAR Institute, Quartier Agora—Allée du six Août, 19c B-4000, Liége, Belgium
[3] Department of Physics, The Ohio State University, Columbus, OH 43210, USA
[4] Center for Cosmology and Astro-Particle Physics, The Ohio State University, Columbus, OH 43210, USA
[5] Kavli Institute for Cosmological Physics, University of Chicago, Chicago, IL 60637, USA
[6] Fermi National Accelerator Laboratory, P.O. Box 500, Batavia, IL 60510, USA
[7] Department of Astronomy and Astrophysics, University of Chicago, Chicago, IL 60637, USA
[8] Institute of Physics, Laboratory of Astrophysics, Ecole Polytechnique Fédérale de Lausanne (EPFL), Observatoire de Sauverny, 1290 Versoix, Switzerland
[9] European Southern Observatory, Alonso de Córdova 3107, Vitacura, Santiago, Chile
[10] ICC-UB Institut de Ciéncies del Cosmos, University of Barcelona, Martí Franqués, 1, E-08028 Barcelona, Spain
[11] ICREA, Pg. Lluís Companys 23, Barcelona, E-08010, Spain
[12] Instituto de Astrofisica, Universidad Andrés Bello, Fernández Concha 700, 7591538 Santiago de Chile, Chile
[13] Max-PlanckInstitute for Astronomy, Königstuhl 17, D-69117 Heidelberg, Germany
[14] Kavli Institute for Particle Astrophysics and Cosmology, Stanford University, Stanford, CA 94305, USA
[15] Department of Physics, Stanford University, 382 Via Pueblo Mall, Stanford, CA 94305, USA
[16] Department of Physics and Astronomy, University of California, Los Angeles, CA 90095, USA
[17] Center for Astrophysical Surveys, National Center for Supercomputing Applications, 1205 West Clark St., Urbana, IL 61801, USA
[18] Centro Brasileiro de Pesquisas Físicas, Rua Dr, Xavier Sigaud 150, Rio de Janeiro, RJ, Brazil
[19] Instituto de Alta Investigación, Universidad de Tarapacá, Casilla 7D, Arica, Chile
[20] Department of Physics, University of Wisconsin-Madison, Madison, WI 53706, USA
[21] ASTRAVEO, LLC, P.O. Box 1668, Gloucester, MA 01931, USA
[22] Applied Materials, Inc., 35 Dory Rd., Gloucester, MA 01930, USA
[23] NSF's NOIRLab, 670 N. A'ohoku Pl., Hilo, HI 96720, USA
[24] NSF's NOIRLab, Casilla 603, La Serena, Chile
[25] Department of Physics and Astronomy, Dartmouth College, Hanover, NH 03755, USA
[26] Department of Physics, University of Surrey, Stag Hill Campus, Guildford, GU2 7XH, UK
[27] McWilliams Center for Cosmology, Carnegie Mellon University, 5000 Forbes Ave., Pittsburgh, PA 15218, USA
[28] Center for Astrophysics and Space Astronomy, University of Colorado Boulder, 389 UCB, Boulder, CO 80309, USA
[29] Space Telescope Science Institute, 3700 San Martin Dr., Baltimore, MD 21218, USA
[30] Cerro Tololo Inter-American Observatory/NSF's NOIRLab, Casilla 603, La Serena, Chile
Received 2024 April 21; revised 2025 September 7; accepted 2025 September 8; published 2025 September 29

Abstract

A quadruply lensed source, J125856.3–031944, has been discovered using the DELVE survey and Wide-field Infrared Survey Explorer W1–W2 colors. Follow-up direct imaging carried out with the Magellan Baade 6.5 m telescope is analyzed, as is spectroscopy from the 2.5 m Nordic Optical Telescope. The lensed image configuration is kite-like, with the major axis of the lensing galaxy along the symmetry axis of the kite, and with the faintest image at its tail. Redward of 6000 Å, the tail image is strongly blended with the lensing galaxy. The Sloan *g* direct imaging carried out with Magellan permits deblending. As the lensed image configuration is nearly circular, simple models give high predicted magnifications for all four images. The source's narrow emission lines at redshift $z = 2.225$ and low intrinsic luminosity qualify it as a type 2 active galactic nucleus. The Magellan image shows a substantial residual that suggests a second lensing galaxy.

Unified Astronomy Thesaurus concepts: Low-luminosity active galactic nuclei (2033); Quasars (1319); Strong gravitational lensing (1643)

1. Introduction

Quadruply lensed quasar systems are routinely used to study the lensing galaxies (S. Vegetti et al. 2024), the quasars themselves (G. Vernardos et al. 2024), and the geometry of the Universe through which their light propagates (T. Treu & P. J. Marshall 2016). But they are rare, both because quasars are themselves rare and because they have only a $\mathcal{O}(10^{-4})$ chance of being quadruply lensed (M. Oguri & P. J. Marshall 2010). Worse yet, several observational considerations make them difficult to identify, the most important of which is their small angular extent on the sky, $\sim 1''$.

Here we report the discovery of the first confirmed quadruply lensed active galactic nucleus (AGN) found in the

DELVE Quadruply Lensed Quasar (henceforth DELQQ) survey, carried out in the DELVE footprint (A. Drlica-Wagner et al. 2021), using the Dark Energy Camera (DECam) at the Victor M. Blanco 4 m telescope (B. Flaugher et al. 2015). J125856.3–031944 (henceforth DELQQ 1258–0319) presents several challenges. Foremost among these, the lensing galaxy overlaps with several of the images, making deblending difficult. Using only the original survey data, we could not thoroughly convince ourselves that the system was indeed quadruple, and not a "naked cusp" configuration like that of J0457–7820 (C. Lemon et al. 2022), because the faintest quasar image is too close to the lensing galaxy.

In higher resolution follow-up data, there appears to be a second lensing galaxy that lies close to two of the brighter images, complicating modeling of the system. The image configuration is nearly circular, so small uncertainties in the image positions produce large changes in the resulting models (C. Falor & P. L. Schechter 2022).

As deeper ground-based surveys are carried out, most recently DELVE (A. Drlica-Wagner et al. 2021) and soon, the Legacy Survey of Space and Time (Ž. Ivezić et al. 2019), quadruple quasars with increasingly faint images relative to the galaxies that lens them will become more prevalent, and their modeling may be similarly challenging.

2. Discovery

2.1. The DELQQ Survey: Selection

Our survey, which we call DELQQ, covered the 6000 deg^2 of the first DELVE data release (A. Drlica-Wagner et al. 2021). Details of the survey are given in Appendix A. Candidate quasars with color W1 − W2 > 0.7 and W1 < 15.5 as measured by the Wide-field Infrared Survey Explorer (WISE; E. L. Wright et al. 2010) satellite were chosen following the color criterion proposed by D. Stern et al. (2012), for a total of 150,000 sources. Square FITS cutouts, 45 pixels (∼11.″85) on a side, were then generated for those candidates from the DELVE survey g, r, i, and z images.

A still-evolving computer program, `trifurcator`, first described in P. L. Schechter et al. (2018), was used to split sources into three components, which were classified as pointlike, $\mathcal{P}$, galaxy-like, $\mathcal{G}$, or ambiguous, $\mathcal{Q}$. Systems for which none of the components were pointlike were eliminated.

Cutouts in all four filters were visually inspected by the first author for systems in which two components (one of which was pointlike) had near-identical $g - r$, $r - i$, and $i - z$ colors, excluding those whose colors were galaxy-like. Roughly 1500 systems were visually inspected. `Trifurcator` is described in greater detail in Appendix B.

Five quadruply lensed quasars with W1 − W2 > 0.7 had previously been identified in our DELQQ sample, of which `trifurcator` recovered three: J1131–4419 (L. Delchambre et al. 2019), J1134–2103 (J. R. Lucey et al. 2018), and J1131-1231 (D. Sluse et al. 2003). The largest image separations for the two systems not recovered were 0.″66 for B1113–0641 (J. A. Blackburne et al. 2008) and 10″ for J1651–0417 (D. Stern et al. 2021), which were either too close to be resolved by DECam or too widely separated for our search. One known quad J1606–2333 (L. Delchambre et al. 2019) lacked an r exposure. As of the submission of this paper, we were unaware of any other quadruply lensed systems discovered within the DELVE footprint.

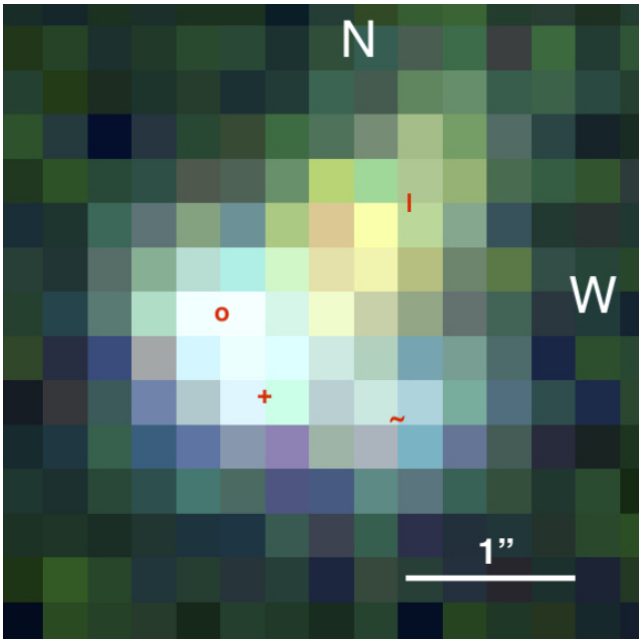

Figure 1. A color composite representation of DELQQ 1258–0319 taken with DECam on the Blanco Telescope, using DES r, i, and z exposures (for blue, green, and red) taken as part of the DELVE survey. The approximate positions of four images subsequently labeled A, B, C, and D are shown in red with the symbols ∘, +, ∼, and |, respectively.

2.2. A Candidate

Only one candidate emerged as a possible quadruply lensed quasar system, DELQQ J1258–0319. A color image generated from the DELVE r, i, and z exposures is shown in Figure 1.

`Trifurcator` split the r exposure into three components: a pointlike $\mathcal{P}$ component to the southwest, marked by a red "∼" in Figure 1, and two extended, galaxy-like $\mathcal{G}$ components, one centrally located (a blend of an apparent lensing galaxy and an image marked by the symbol "|") and one toward the east (a blend of two images of the source marked by the symbols "∘" and "+"). The colors of this blend agree with those of the pointlike object with an rms of 0.14 magnitudes, after allowing for a modest slope due to microlensing, extinction, and point-spread function (PSF) mismatch. They were flagged as possible components of a quadruply lensed quasar. The central galaxy-like component has much redder colors.

The program assigned a DELVE g magnitude of 22.68 to the pointlike image and $g - r$, $r - i$, and $i - z$ colors of 0.373, 0.279, and 0.291, respectively. The latter are useful for establishing achromaticity but less so for deriving quasar properties, as the exposures spanned five observing seasons.

While it was possible to split the central component into two point sources, one of which would be a fourth quasar image, we could not persuade ourselves that the data justified this.

A program called `clumpfit`, described in Appendix C, was used to fit five point sources simultaneously. Though the decomposition of the two $\mathcal{G}$ images into point sources did give positions that were in qualitative agreement with expectations for a quadruply lensed source, reasonable alternative choices of possible PSFs produced large deviations from these positions.

2.3. Prior Detections

Prior to its detection in DELVE, DELQQ J1258–0319 had been cataloged as a source both in the Pan-STARRS catalog

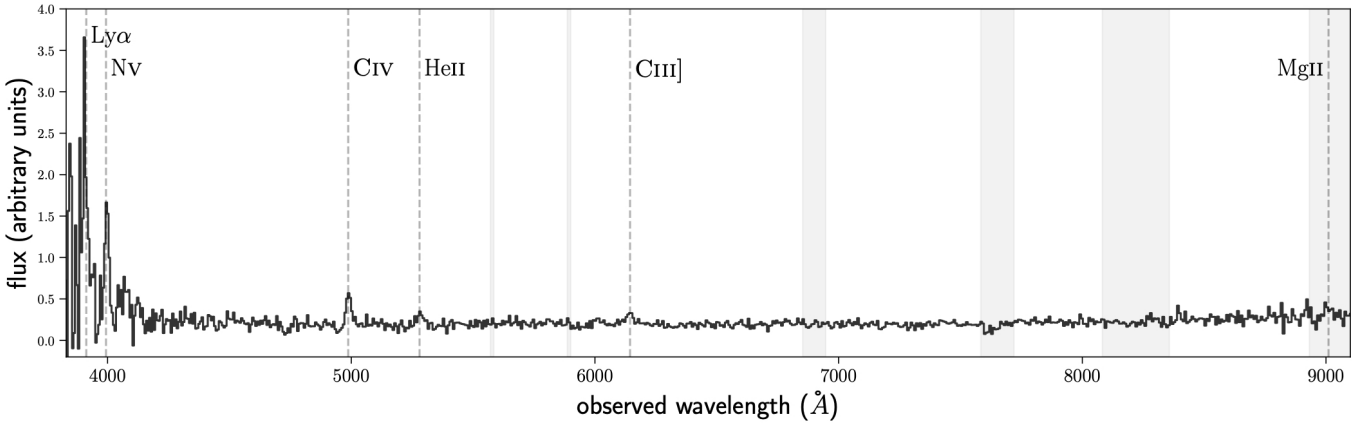

Figure 2. NOT spectrum of the brightest quasar component *A*, extending from 3800 to 9000 Å. The high ionization lines of N V, C IV, and He II seen at $z = 2.225$ are narrow, with widths ranging from 1300 to 2000 km s^{-1}, suggesting a type 2 AGN rather than a quasar.

(K. C. Chambers et al. 2016) and the VLASS (M. Lacy et al. 2020). Its nondetection in Gaia DR2 indicates that it is substantially fainter than the large majority of known quadruply lensed quasars.

3. Follow-up MPIA-Wide Field Imager Imaging

Four Cousins R_c follow-up exposures of 320 s each were obtained with the Wide Field Imager of the MPIA 2.2 m telescope on La Silla in seeing of roughly 0.″64. Notwithstanding the good seeing and pixels of 0.″238, there was no clear separation of the lensing galaxy and the faintest of the quasar images. Attempts by two of the authors to determine the ellipticity of the lensing galaxy using differing techniques yielded substantially different results.

4. Follow-up Nordic Optical Telescope Spectroscopy

A 40 minute spectrum was obtained with the Alhambra Faint Object Spectrograph and Camera on the Nordic Optical Telescope (NOT) on 2021 April 16. The slit was oriented so as to pass through the brightest of the four images and the lensing galaxy. A spectrum extracted at the position of the image "○" is shown in Figure 2. Narrow emission lines are clearly visible, corresponding to a redshift $z = 2.225$.

A sharp discontinuity in the galaxy spectrum is seen in the original two-dimensional spectrum at 6000 Å, suggestive of the *H and K* break in early-type galaxies. In Section 5 below, we use astrometry obtained with Magellan's Walter Baade telescope to force photometry on the original DELVE data and obtain colors for the lensing galaxy. The resulting photometric redshift is consistent with this interpretation.

5. Follow-up Magellan IMACS Imaging

5.1. 2022 May

Three 300 s exposures of DELQQ J1258–0319 in each of the Sloan *g* and *i* filters were obtained with the IMACS *f*/4 camera (A. Dressler et al. 2011) on the Baade 6.5 m telescope of the Magellan Observatory on 2022 May 24, at a scale of 0.″111 per pixel. These sufficed to distinguish the fourth image, "|," from the much redder lensing galaxy, and to get positions for each of them. Attempts to determine the shape of the lensing galaxy were inconclusive, as it blended with the three bright quasar images.

5.2. 2024 July

Three IMACS 300 s exposures of DELQQ J1258–0319 in the Sloan *g* filter were obtained on 2024 July 6, a coaddition of which is shown in Figure 3(a). These had better seeing than the 2022 May images. A nearby star ($\alpha = 194.7527$, $\delta = -3.3168$) was used to construct an empirical PSF, which was then fitted to the four quasar images *and* to the lensing galaxy, again using `clumpfit`, described in Appendix C. As with the earlier IMACS data, overlap between the galaxy and the quasar images precluded the determination of the shape or size of the lensing galaxy.

Residuals obtained by subtracting five point sources from the stacked image are shown in Figure 3(b). There is a bright spot (which is dark on our inverted color map) between quasar images *B* and *C*, which we call *E*. Treating this as a sixth point source gives the very much improved residuals shown at the same contrast in Figure 3(d). The positions of the four quasar images showed appreciable shifts from Figure 3(c).

Fits of a singular isothermal elliptical potential (SIEP) model to these new positions, described in Section 6 below, produced a χ^2 smaller by a factor of $(4.7)^2$ than did fits to the positions of Figure 3(c). We take this as strong evidence that *E* is a second lens rather than a fifth image of the source.

The Magellan *g* images were taken in nonphotometric conditions. The DELVE catalog mean magnitude for the empirical PSF star is $g = 20.322$, which gives $g = 24.53 \pm 0.05$ for the lensing galaxy. The Magellan positions for the six point sources in Figure 3(c) were forced onto the original *r*, *i*, and *z* DELVE images, using the DELVE PSFs, to give photometry for the lensing galaxy. Combining these with the Magellan *g* magnitude, we assign colors to the lensing galaxy of $g - r = 2.17$, $r - i = 1.60$, and $i - z = 0.55$, treating it as a point source.

We obtained a photometric redshift using `Bayesian Photometric Redshift` (hereafter BPZ) described by N. Benítez (2000) and D. Coe et al. (2006). Prior distributions were derived from Hubble Deep Field North galaxies. We ran BPZ with the point-source fit apparent magnitudes given in Table 1. We took the photometric uncertainty to be ±0.05 mag in Magellan *g*, which is the formal error reported from the `clumpfit` covariance matrix for objects *A*–*E* and *G*, with positions taken to be free. We took it to be ±0.07, ±0.05, and ±0.04 in *r*, *i*, and *z*, respectively, which are the formal errors reported from the `clumpfit` covariance matrices from the forced fits to the individual DELVE cutouts.

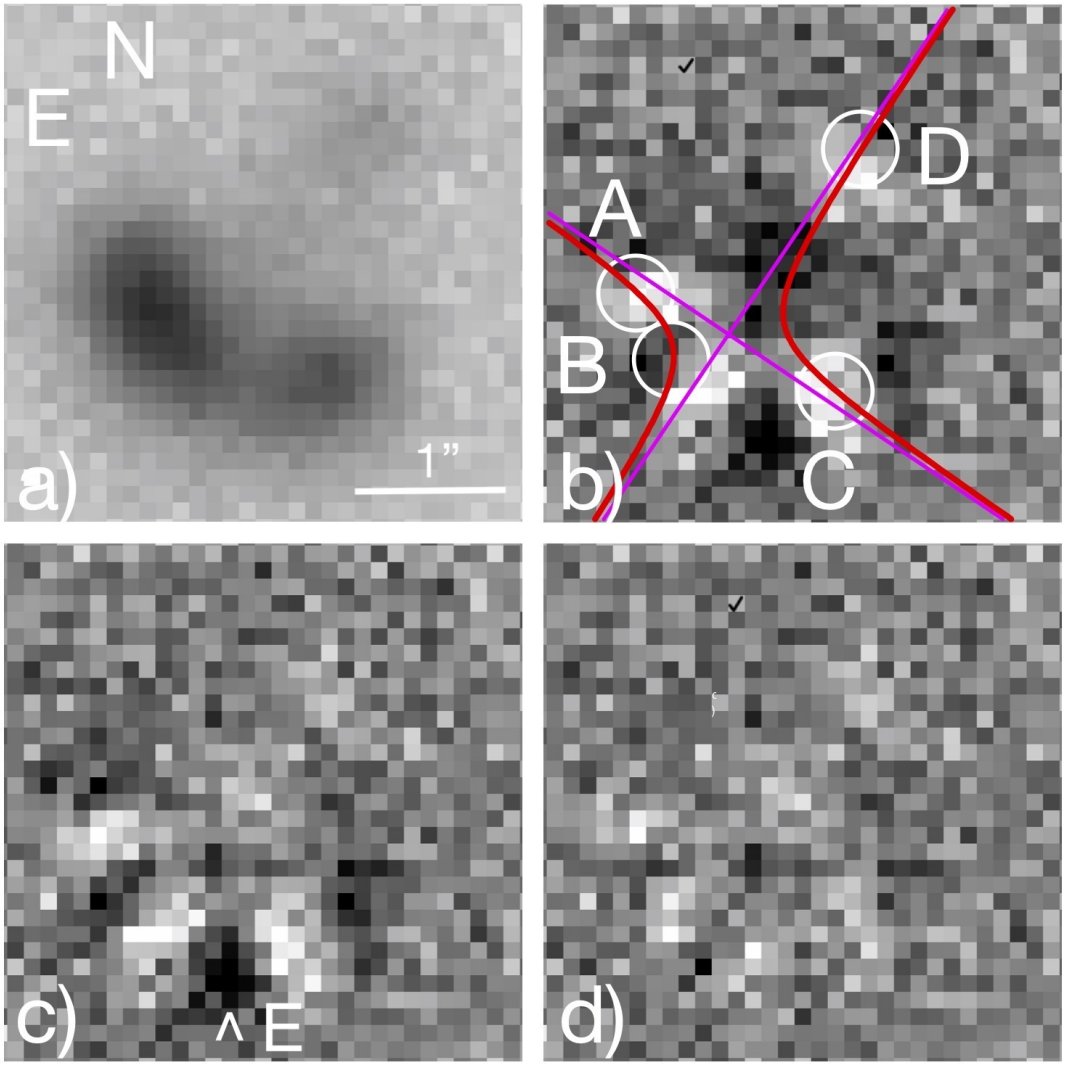

Figure 3. (a) DELQQ 1258–0319 observed with a Sloan g filter for 900 s with the IMACS $f/4$ camera on the Magellan Baade telescope. A negative grayscale is used to highlight the low surface brightness of the central lens, which is substantially fainter than the four images surrounding it. (b) Four point sources, A, B, C, and D, have been fitted and subtracted. A rectangular hyperbola (red) has been drawn through the fitted positions. According to H. J. Witt (1996), if the potential is elliptical, the hyperbola's asymptotes (magenta) are parallel to its major and minor axes, and the lensing galaxy must lie on the longer, primary branch of the hyperbola. A faint source, which we take to be the lensing galaxy, is consistent with Witt's prediction. (c) A point source has been fitted to the lensing galaxy, which is too faint to permit determination of its extent. White regions indicate oversubtraction of the point sources. (d) A substantial residual southeast of image C, which we call E, has been fitted by a point source and subtracted. The positions from this fit are shown in panel (b) as white circles.

The best-fit redshift was found to be $z_{\rm lens} = 0.90 \pm 0.06$. Multiple experiments were carried out exploring possible systematic effects in the magnitudes and the effects of underestimating the uncertainties, among them increasing our adopted errors by factors of 2 and 4. In all but the most extreme cases, the results were consistent with the best fit.

6. Lens Models

We used Keeton's `lensmodel` program (C. R. Keeton 2010) to model the positions of the quasar images shown by the white circles in Figure 3(c) and given in Table 1. The lensing galaxy was represented as a SIEP,

$$\psi(b, q_{\rm pot}) = b\sqrt{q_{\rm pot}x^2 + \frac{y^2}{q_{\rm pot}}}. \quad (1)$$

Here, ψ is the dimensionless projected potential and $q_{\rm pot}$ is the axis ratio of this potential (rather than that of its surface mass density).[31] The lens strength b is measured in arcseconds, and gives the Einstein ring radius in the limit of small ellipticities. These were treated as free parameters, as was the position angle (P.A.) of the long axis. The four image positions were assigned uncertainties of $0\farcs01$. Results from this fit are presented in the first line of Table 2. The predicted magnification μ of image C is also given.

The second line in Table 2 models the image positions with both an SIEP and with a singular isothermal sphere (SIS) at the position of point source E. One additional parameter, $b_{\rm sis}$, has improved the mean squared residual of the image positions by

[31] For very round potentials, the underlying mass is roughly 3 times flatter (R. Luhtaru et al. 2021).

Table 1
DELQQ 1258–0319: Astrometric, Photometric, and Modeled Quantities

Image	ΔR.A. (arcsec)	ΔDecl. (arcsec)	g	$g - i$[a]	F_g (nJy)	μ	κ[b]	Δt (days)
A	0.96	−0.28	22.13	0.91	1405	65.7	0.503	2.52
B	0.72	−0.93	23.06	1.13	964	−190.	0.526	2.62
C	−0.37	−0.94	22.46	1.21	847	8.7	0.467	0.00
D	−0.54	0.68	23.02	1.64	620	−5.7	0.587	24.0
E	0.17	1.10	23.25	1.38	501	…	…	…
G	0.00	0.00	23.52	2.74	…	…	…	…

Notes.
[a] Colors assume a pointlike lens. Extended flux from the much redder lens contaminates the colors of $A - E$.
[b] For an SIEP, shear $\gamma =$ convergence κ.

Table 2
Model Fits to Image Positions

Model	$b_{\rm siep}$	$b_{\rm sis}$	$\epsilon_{\rm siep}$	P.A.[a] (deg)	μ_C	χ^2
SIEP	0.″97	…	0.020	−33	34	87
SIEP + SIS	0.″93	0.″03	0.045	−45	9	4

Note.
[a] Position angles are measured from east to north.

a factor of $(4.67)^2$. Yet more remarkably, the strength of the added SIS is a very small fraction, $1/30$, of that of the SIEP.

C. Falor & P. L. Schechter (2022) show that for asymptotically circular quads, the magnification of the closest pair of images increases inversely as their separation. The SIEP centered on the lensing galaxy has an ellipticity $\epsilon_{\rm siep}$ of just 0.045, so even a small perturbation can have a large effect on the close pair.[32] Our hypothesized perturber at position E in Figure 3(c) pushes image B closer to image A. C. Falor and P. L. Schechter (2022) also found that for asymptotically circular quads, the absolute magnifications for all four images vary inversely with the ellipticity of the potential.

We have chosen to give the predicted magnification for image C in Table 2 because (as the leading image in Table 1) it is the least subject to changes in the lensing potential. The predicted flux ratios in Table 1 A/C and B/C are 22 and 7, substantially higher than the observed ratios of 1.7 and 1.1, respectively.

L. Weisenbach et al. (2021) have shown that such large deviations from predicted fluxes are unlikely to be the result of gravitational microlensing. Nor do we think it is due to the obscuration of image C by dust, as its $g - i$ colors are no different from those of A and B.

We believe, instead, that the unusual flux ratios reflect a shortcoming of our observations. The lensing galaxy appears to be elongated roughly along an axis from image D to image A. In models that take the stellar axis ratio of the lens to be a free parameter, it is strongly degenerate with the positions of those two images. Plausible changes in the image positions could produce different modeled flux ratios, but would not be sufficiently large to change the near-circular character of the potential.

[32] R. Luhtaru et al. (2021) find a typical ellipticity for the potentials of quadruply lensed quasars of 0.21.

7. Quasar, LLAGN, or Seyfert?

Based on the narrow emission lines seen in Figure 2, E. E. Khachikian & D. W. Weedman (1971) and E. Y. Khachikian & D. W. Weedman (1974)—the first of these in Russian and the second in English—would have classified the source in DELQQ 1258–0319 as a Seyfert II galaxy rather than a Seyfert I or a quasar. Subsequent work indicated that the physics of the AGNs of such systems is somewhat decoupled from the properties of the galaxies that host them. In a review of "unified models," R. Antonucci (1993) presents a cartoon model in which type 2 AGNs have narrow emission lines with FWHM $\mathcal{O}(1000)$ km s^{-1}, and type 1 AGNs have broad emission lines with FWHM $\mathcal{O}(10,\,000)$ km s^{-1}. Such systems are classified as Seyferts only if the host galaxy is observed, which may eventually happen if the system is observed at sufficiently high spatial resolution and surface brightness sensitivity.

The source in the DELQQ 1258–0319 system is not very red, as would have been the case if dust were obscuring both its broad line region and continuum emission from its accretion disk. The high magnifications derived from our models and the photometry from the original DELVE images point to a source absolute magnitude M_{AB} fainter than those of the low-luminosity quasars in the SHELLQs survey (Y. Matsuoka et al. 2016). It would therefore seem that the first quadruply lensed AGN in the DELVE Quadruple Quasar survey does not qualify as a quasar. As we do not, as yet, see evidence of the host galaxy, the source is classified as a low-luminosity AGN—"LLAGN"—and not a Seyfert.

8. Conclusions

With the benefit of hindsight, none of the challenges described in the preceding sections is entirely surprising. Many of the brighter quadruply imaged quasars with wider separations have already been discovered, particularly since the publication of Gaia DR2 (L. Delchambre et al. 2019; C. Lemon et al. 2022). The W2 − W1 > 0.7 criterion will not be satisfied by systems for which the lensing galaxy contributes a substantial fraction of the infrared light. Lensed image configurations often include faint images like D (the highest saddlepoint of the light travel time) lying relatively close to the lensing galaxy, making deblending more difficult. Seyfert galaxies are more common than quasars (C. J. Willott et al. 2000), and may account for an increasingly large fraction of quadruply lensed sources in future surveys that push to fainter apparent magnitudes. And at fainter apparent magnitudes,

it may not be possible to deblend the targets into at least three images in all four filters, as described in Appendix B. Direct forward lens modeling of the pixels, rather than identifying $\mathcal{P}, \mathcal{G}$, and $\mathcal{Q}$ components of the system in multiple filters, would permit quads to be identified in a single filter.

The preceding sections reveal an as yet unquenched thirst for higher and yet higher resolution, first to confirm that the AGN DELQQ 1258–0319 is in fact quadruply lensed and then to separate its multiple images from the lensing galaxy, which would appear to have a companion. One might do yet better from the ground with "lucky imaging" (N. M. Law et al. 2006), but bright nearby stars usually needed for adaptive optics are scarce.

Beyond that, one must get above the Earth's atmosphere. In the time since this paper was first submitted, DELQQ 1258–0319 was included in a successful Hubble Space Telescope "bridge" program, which may help resolve some of the outstanding questions.

Acknowledgments

We warmly thank R. Gredel, H.-W. Rix, and T. Henning for allowing us to observe with the MPIA 2.2 m telescope. We thank N. Zakamska for an extended disquisition on the physics underlying the arcana of AGN classification. We thank an anonymous referee whose suggestions for clarification precipitated the inclusion of the supplementary material in Appendices A–C. This program has been supported in part by the Swiss National Science Foundation (SNSF) and by the European Research Council (ERC) under the European Union's Horizon 2020 research and innovation program (COSMICLENS: grant agreement No. 787886). M.M. acknowledges the support of the Swiss National Science Foundation (SNSF) under grant P500PT203114. T.T. acknowledges support by the NSF through grants 1906976 and 1836016. The authors acknowledge the award of telescope time for the DELVE project (2019A-0305; PI: Drlica-Wagner) by NSF's NOIRLAB, which is operated by the Association of Universities for Research in Astronomy (AURA) under a cooperative agreement with the National Science Foundation.

Funding for the DES Projects has been provided by the U.S. Department of Energy, the U.S. National Science Foundation, the Ministry of Science and Education of Spain, the Science and Technology Facilities Council of the United Kingdom, the Higher Education Funding Council for England, the National Center for Supercomputing Applications at the University of Illinois at Urbana-Champaign, the Kavli Institute of Cosmological Physics at the University of Chicago, the Center for Cosmology and Astro-Particle Physics at the Ohio State University, the Mitchell Institute for Fundamental Physics and Astronomy at Texas A&M University, Financiadora de Estudos e Projetos, Fundação Carlos Chagas Filho de Amparo á Pesquisa do Estado do Rio de Janeiro, Conselho Nacional de Desenvolvimento Científico e Tecnológico and the Ministério da Ciência, Tecnologia e Inovacão, the Deutsche Forschungsgemeinschaft, and the Collaborating Institutions in the Dark Energy Survey.

Facilities: Blanco (DECcam), Max Planck:2.2m (WFI), NOT (ALFOSC), Magellan:Baade (IMACS)

Appendix A
Description of the Delve Survey

We quote verbatim the abstract of A. Drlica-Wagner et al. (2021) describing DELVE.

The DECam Local Volume Exploration survey (DELVE) is a 126-night survey program on the 4 m Blanco Telescope at the Cerro Tololo Inter-American Observatory in Chile. DELVE seeks to understand the characteristics of faint satellite galaxies and other resolved stellar substructures over a range of environments in the Local Volume. DELVE will combine new DECam observations with archival DECam data to cover roughly $\sim$15,000 deg^2 of high Galactic latitude ($|b| > 10$ deg) southern sky to a 5σ depth of $g, r, i, z \sim 23.5$ mag. In addition, DELVE will cover a region of 2200 deg^2 around the Magellanic Clouds to a depth of $g, r, i \sim 24.5$ mag and an area 135 deg^2 around four Magellanic analogs to a depth of $g, i \sim 25.5$ mag. Here, we present an overview of the DELVE program and progress to date. We also summarize the first DELVE public data release (DELVE DR1), which provides point-source and automatic aperture photometry for roughly 520 million astronomical sources covering roughly 5000 deg^2 of the southern sky to a 5σ point-source depth of $g = 24.3$ mag , $r = 23.9$ mag, $i = 23.3$ mag, and $z = 22.8$ mag. DELVE DR1 is publicly available via the NOIRLab Astro Data Lab science platform.

Of particular relevance for the present work, the DELVE survey uses `PSFeX` (E. Bertin 2011) to produce a tabulated PSF at any desired position. As illustrated in Figure 2 of A. Drlica-Wagner et al. (2021), the median PSF FWHM ranged from $\sim$1.″0 in z to $\sim$1.″25 in g and was properly sampled by DECam's 0.″263 pixels.

Appendix B
How `Trifurcator` Works

A still-evolving program, `trifurcator`, was used to select candidates from our WISE targets. The program deblends images in all four DELVE filters for each of the WISE targets into three components using an algorithm drawn from `DoPHOT` (P. L. Schechter et al. 1993), classifying the components as either pointlike or extended, using the DELVE PSF as a reference. It then requires that at least one pointlike component has quasar-like colors drawn from Table 3 of G. T. Richards et al. (2001) and that a second component has colors identical to the pointlike component. The second component need not be pointlike, as it may be an unresolved blend of two quasar images. Systems for which none of the components are pointlike in any of the filters are eliminated.

If these criteria are satisfied in any one of the DELVE filters, the three components are used to force photometry on the other DELVE filters using the empirical PSF option in `DoPHOT`.

Cutouts in all four filters are then visually inspected for systems in which two components (one of which was pointlike) had near-identical $g - r$, $r - i$, and $i - z$ colors, with a scatter less than 0.2 mag. If these colors were galaxy-like, the system was dropped from further consideration. Roughly 1500 systems were visually inspected by the first author.

In an experiment (to be reported elsewhere) conducted by two of the present authors, two dozen individuals with considerable lensing experience were shown the image configurations for three of the four images of known quasars

and asked to mark the position of the fourth. They did so with high reliability, and in some cases identified reasonable alternative positions. The results instill a measure of confidence in the present visual inspections.

Appendix C
How `Clumpfit` Works

Like `trifurcator`, `clumpfit` uses pieces of the program `DoPHOT` (P. L. Schechter et al. 1993) to obtain parameters for pointlike and extended sources in a cutout. Initial positions, and for extended sources, initial shape parameters are specified and then simultaneously adjusted to obtain a best fit. One can either let the program solve for an analytic PSF or specify a PSF. For the original DELVE cutouts, the DELVE PSF was used. For the Magellan IMACS data, a nearby star was used as a pixelated template. The program has much in common with `GALFIT` (C. Y. Peng et al. 2010).

ORCID iDs

Paul L. Schechter https://orcid.org/0000-0002-5665-4172
Dominique Sluse https://orcid.org/0000-0001-6116-2095
Erik A. Zaborowski https://orcid.org/0000-0002-6779-4277
Alex Drlica-Wagner https://orcid.org/0000-0001-8251-933X
Cameron Lemon https://orcid.org/0000-0003-2456-9317
Frederic Dux https://orcid.org/0000-0003-3358-4834
Frederic Courbin https://orcid.org/0000-0003-0758-6510
Angela Hempel https://orcid.org/0000-0002-6315-3085
Martin Millon https://orcid.org/0000-0001-7051-497X
Tommaso Treu https://orcid.org/0000-0002-8460-0390
Raul Teixeira https://orcid.org/0000-0002-5279-0230
Monika Adamów https://orcid.org/0000-0002-6904-359X
Clecio R. Bom https://orcid.org/0000-0003-4383-2969
Julio A. Carballo-Bello https://orcid.org/0000-0002-3690-105X
Peter S. Ferguson https://orcid.org/0000-0001-6957-1627
Robert A. Gruendl https://orcid.org/0000-0002-4588-6517
David J. James https://orcid.org/0000-0001-5160-4486
Clara E. Martínez-Vázquez https://orcid.org/0000-0002-9144-7726
Pol Massana https://orcid.org/0000-0002-8093-7471
Sidney Mau https://orcid.org/0000-0003-3519-4004
Burçin Mutlu-Pakdil https://orcid.org/0000-0001-9649-4815
Noëlia E. D. Noël https://orcid.org/0000-0002-8282-469X
Andrew B. Pace https://orcid.org/0000-0002-6021-8760
Joanna D. Sakowska https://orcid.org/0000-0002-1594-1466
Guy S. Stringfellow https://orcid.org/0000-0003-1479-3059
Erik J. Tollerud https://orcid.org/0000-0002-9599-310X
A. Katherina Vivas https://orcid.org/0000-0003-4341-6172
Alfredo Zenteno https://orcid.org/0000-0001-6455-9135

References

Antonucci, R. 1993, ARA&A, 31, 473
Benítez, N. 2000, ApJ, 536, 571
Bertin, E. 2011, in ASP Conf. Ser. 442, Astronomical Data Analysis Software and Systems XX, ed. I. N. Evans et al. (San Francisco, CA: ASP), 435
Blackburne, J. A., Wisotzki, L., & Schechter, P. L. 2008, AJ, 135, 374
Chambers, K. C., Magnier, E. A., Metcalfe, N., et al. 2016, arXiv:1612.05560
Coe, D., Benítez, N., Sánchez, S. F., et al. 2006, AJ, 132, 926
Delchambre, L., Krone-Martins, A., Wertz, O., et al. 2019, A&A, 622, A165
Dressler, A., Bigelow, B., Hare, T., et al. 2011, PASP, 123, 288
Drlica-Wagner, A., Carlin, J. L., Nidever, D. L., et al. 2021, ApJS, 256, 2
Falor, C., & Schechter, P. L. 2022, AJ, 164, 120
Flaugher, B., Diehl, H. T., Honscheid, K., et al. 2015, AJ, 150, 150
Ivezić, Ž., Kahn, S. M., Tyson, J. A., et al. 2019, ApJ, 873, 111
Keeton, C. R. 2010, GReGr, 42, 2151
Khachikian, E. E., & Weedman, D. W. 1971, Afz, 7, 389
Khachikian, E. Y., & Weedman, D. W. 1974, ApJ, 192, 581
Lacy, M., Baum, S. A., Chandler, C. J., et al. 2020, PASP, 132, 035001
Law, N. M., Mackay, C. D., & Baldwin, J. E. 2006, A&A, 446, 739
Lemon, C., Anguita, T., Auger-Williams, M. W., et al. 2022, MNRAS, 520, 3305
Lucey, J. R., Schechter, P. L., Smith, R. J., & Anguita, T. 2018, MNRAS, 476, 927
Luhtaru, R., Schechter, P. L., & de Soto, K. M. 2021, ApJ, 915, 4
Matsuoka, Y., Onoue, M., Kashikawa, N., et al. 2016, ApJ, 828, 26
Oguri, M., & Marshall, P. J. 2010, MNRAS, 405, 2579
Peng, C. Y., Ho, L. C., Impey, C. D., & Rix, H.-W. 2010, AJ, 139, 2097
Richards, G. T., Fan, X., Schneider, D. P., et al. 2001, AJ, 121, 2308
Schechter, P. L., Anguita, T., Morgan, N. D., Read, M., & Shanks, T. 2018, RNAAS, 2, 21
Schechter, P. L., Mateo, M., & Saha, A. 1993, PASP, 105, 1342
Sluse, D., Surdej, J., Claeskens, J. F., et al. 2003, A&A, 406, L43
Stern, D., Assef, R. J., Benford, D. J., et al. 2012, ApJ, 753, 30
Stern, D., Djorgovski, S. G., Krone-Martins, A., et al. 2021, ApJ, 921, 42
Treu, T., & Marshall, P. J. 2016, A&ARv, 24, 11
Vegetti, S., Birrer, S., Despali, G., et al. 2024, SSRv, 220, 58
Vernardos, G., Sluse, D., Pooley, D., et al. 2024, SSRv, 220, 14
Weisenbach, L., Schechter, P. L., & Pontula, S. 2021, ApJ, 922, 70
Willott, C. J., Rawlings, S., Blundell, K. M., & Lacy, M. 2000, MNRAS, 316, 449
Witt, H. J. 1996, ApJL, 472, L1
Wright, E. L., Eisenhardt, P. R. M., Mainzer, A. K., et al. 2010, AJ, 140, 1868